Apertureless Near-Field Optical Microscopy for Pristine Materials - Much Higher Resolution Below Diffraction Limit and Versatility than Stochastic Techniques

Kaupp Gerd*

University of Oldenburg, Oldenburg, Lower Saxony, Germany

Abstract

The strong enhancement of the reflection back to the sharp (R<20 nm) tapered quartz tip (factor >2 up to 50!) uniquely enables apertureless shear force SNOM, local Raman, and fluorescence of flat or rough daily life and real world surfaces of all types, including biological/medical ones. It is highly versatile, economic, artifact-free at slopes up to 70° (sometimes 80°) with heights of several μm, and uncomplicated. Sharp tips are pulled at almost no cost. The unparalleled optical resolution is <8.6 nm. Also numerous industrial and biological/medical applications are revealed at the several μm ranges, for example cancer detection in up to 25 × 25 μm^2 or up to 50 × 50 nm^2 frames within 2 min. None of these qualities are present in more recent stochastic techniques like STED, STORM, PALM, etc, that must first chemically react biological samples all over with huge fluorescence dyes for detection and calculation of fluorescence distributions at only slight submicroscopic resolution. The ensuing claims of the stochastic work must therefore be counterchecked (this includes creation of improved knowledge) by the revival of save cheap and easy apertureless SNOM revealing much finer details of the actual bio objects in their actual hydrogen bonding and coiling states, for the sake of reality and further progress. Physical foundations and applications in physics, chemistry, biology, medicine, and industry are demonstrated. Nothing of that is achievable by STED, STORM, PALM, etc. with their highly-restricted versatility.

Keywords: Apertureless SNOM; Biomaterials; Cancer detection; Chemical contrast; Industrial applications; Local Raman SNOM; Optical resolution at the nanoscale; Reflection enhancement; Shear force gap; Suborganelle features

Abbreviations: AFM: Atomic force microscopy; BASF: Badische Anilin und Soda Fabrik; BMBF: Bundesministerium für Forschung und Technologie (Federal Ministry for Research and Technology); DME: Danish Micro Engineering A/S (Transformervej 12, 2730 Herlev, Denmark); FKZ: Förderkennzeichen (support number); HE staining: Haematoxylin and eosin staining; TU: Technical University; IBA: Institut für Bioprozess- und Analysenmesstechnik; IFU: Institut für Umweltanalysen; LMT: Lebensmitteltechnologie; NSOM: Near-field scanning optical microscopy; PALM: Photoactivated localization microscopy; PTB: Physikalisch Technische Bundesanstalt; SERS: Surface-enhanced Raman spectroscopy; SNOM: Scanning near-field optical microscopy; STED: Stimulated emission depletion; STORM: Stochastic optical reconstruction microscopy; XPS: X-ray Photoelectron Spectroscopy.

Introduction

Light-microscope resolvability is limited by the Abbe diffraction limit (about λ/2, or 200 nm). Various methods to break that limit with light have been put forward. NSOM (near-field scanning optical microscopy) techniques failed by producing artifacts with hot metal-coated aperture probes and concentrating to edge imaging. Only, apertureless SNOM (scanning near-field optical microscopy) with sharply tapered uncoated dielectric tips with high aspect-ratio were able to yield submicroscopic microscopy with lateral edge resolution (e.g., gratings and vertical sites) below 20 nm and chemical difference resolution below 8.6 nm [1]. This technique uses shear force atomic force microscopes with illuminated tapered sharp tips and relies on an unexpected (even denied) [2] physical effect: the strong reflection enhancement (2 to >50 fold, depending on material) of the light reflected back to the illuminated quartz waveguide. This occurs abruptly when reaching shear force distance, but not with blunt or broken tips as

in Mlynek's group [2]. Different unstained flat or corrugated real-world or biological materials' shear force distance reflectivity (at constant amplitude damping) provide chemical SNOM contrast. Despite the easy, reliable, and versatile SNOM technique more recent stochastic techniques such as STED, PALM, STORM, etc, requiring selective chemical bonding of mostly proteins with fluorescent dyes found more interest [3]. They record slightly submicroscopic fluorescence images (resolution in the 100 nm region) and are difficult and very expensive. It appears that the present hype with these does not sufficiently consider the profound and thorough changes of their objects by such chemical reaction (for example the sample's hydrogen bonding, natural coiling, etc.). Any conclusions on such imaging should therefore be counterchecked by direct apertureless SNOM with concomitant AFM (atomic force microscopy) spectroscopy of the unchanged pristine samples. There is however now the risk that the enhanced reflectance to dielectric sharp tips with the much higher resolving power is forgotten in research funding. This is at the cost of scientifically correct progress and of revealing much smaller details. It is therefore timely to review the more versatile, easy, and cheap direct apertureless SNOM capabilities with its chemical contrast plus concomitant topography, enabling urgent validity check of the stochastic conclusions. Furthermore, only the well-preceding [4-11] apertureless SNOM applies to all

*Corresponding author: Gerd Kaupp, University of Oldenburg, Oldenburg, Lower Saxony, Germany, Tel: 4944868386; Fax: 494486920704; E-mail: gerd.kaupp@uni-oldenburg.de

types of pristine flat or rough surfaces (dielectric, metallic, semi conductive, fluorescing, non-fluorescing, organic, biological, opaque or transparent) at optical resolution down to <8.6 nm, and reflected light diffraction for chemical identification with local fluorescence or Raman or IR spectroscopy. Physical details and already available industrial applications are discussed. These cover nanoparticles, sub-organelle-features, blood-bags, diffusion coefficients, cancer detection/localization, and dental-alloy nanopitting check. Nothing of that is available from the expensive and complicated stochastic techniques.

Materials and Methods - Technical Details of Apertureless SNOM

Apertureless shear force SNOM is an addition to long known shear force AFM that provides concomitant topography and feedback for the SNOM at pre-selected constant amplitude damping of the horizontally vibrating tip. The blueprint is shown in Figure 1, as well as the necessity of using uncoated sharp tips at <10 (typically 5 nm) distance to the surface. Pulled multimode quartz tips (at almost no costs with commercial laser puller) with end radii <10 to 20 nm, but not blunt etched, or broken ones provide the enhanced reflectivity. Only sharp uncoated tips stay cold and can follow topography. The tip vibrates with 5 to 10 nm free amplitude at 100-400 kHz and 5 to 10 nm distance while being constantly damped. Topography up to 70 or 80° slopes does not produce artifacts. Scan rates are between 10 and 120 μm/s at a resolution of 512 × 512 pixel. Dense pores (7 to 8 per 10 μm) of 30 nm Si_3N_4-coated porous silicon were twice reproduced down to 2.5 μm at 50 or 75 μm/s rate without tip abrasion/breakage [12]. The weak He/Ne-laser (λ=632,816 nm) at the vibration edge provided the damping control (not a slow tuning fork) for rapid scanning (less than 2 min per frame). Some of its far-field light may add to the stray light background but stays constant and lacked in the Raman measurements with primary light of 488.0 nm light.

The experimental setup from DME is very simple when compared with the excessively complicated and expensive setup of the stochastic techniques [13]. Figure 2 shows that we need two common tables (not shown the control unit, energy meter, and oscilloscope computer to the
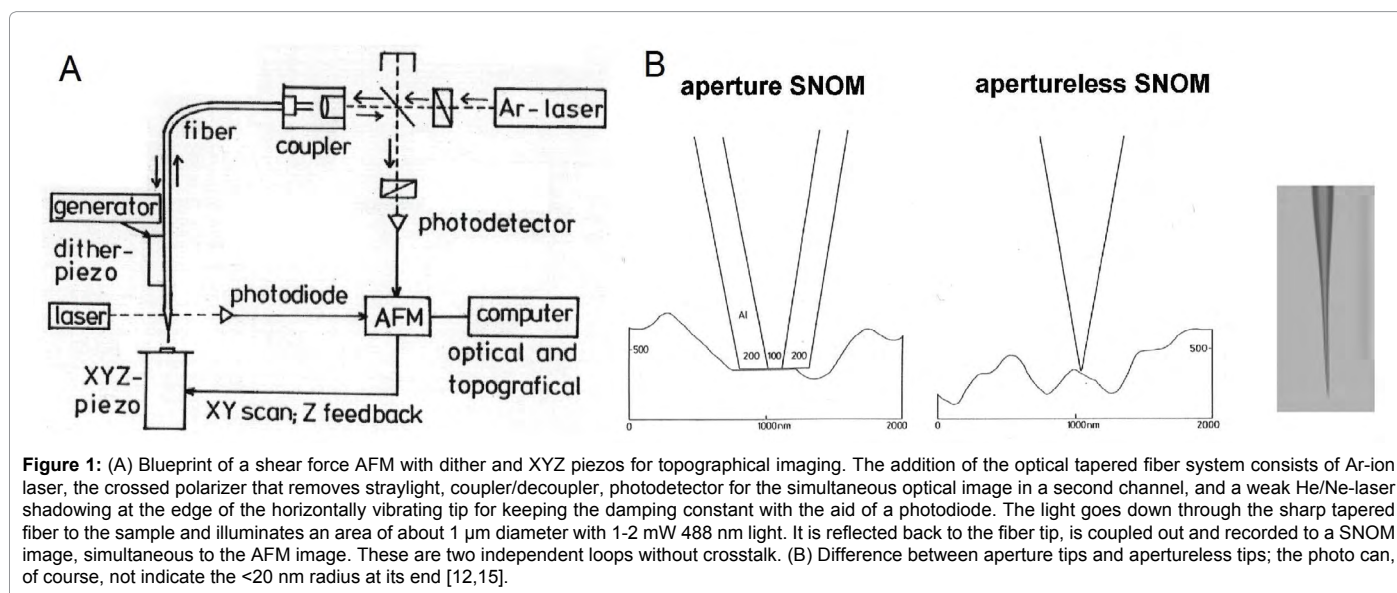

Figure 1: (A) Blueprint of a shear force AFM with dither and XYZ piezos for topographical imaging. The addition of the optical tapered fiber system consists of Ar-ion laser, the crossed polarizer that removes straylight, coupler/decoupler, photodetector for the simultaneous optical image in a second channel, and a weak He/Ne-laser shadowing at the edge of the horizontally vibrating tip for keeping the damping constant with the aid of a photodiode. The light goes down through the sharp tapered fiber to the sample and illuminates an area of about 1 μm diameter with 1-2 mW 488 nm light. It is reflected back to the fiber tip, is coupled out and recorded to a SNOM image, simultaneous to the AFM image. These are two independent loops without crosstalk. (B) Difference between aperture tips and apertureless tips; the photo can, of course, not indicate the <20 nm radius at its end [12,15].

Figure 2: The experimental setup of the shear force AFM/SNOM, here the commercial Rasterscope 4000 of DME with He/Ne-laser damping control [12,15].

right one) and the AFM/SNOM unit hanging on rubber bands to the ceiling for vibration protection. The Ar-ion laser is aligned with a book and paper sheets. The laser coupler with receiver box and hygrometer are enlarged, the fiber between receiver box and scanner is not resolved in the photo.

All artifacts of metal-coated NSOM tips are avoided, and uninterrupted reflected light intensity control secure the valid apertureless SNOM conditions. The enhanced reflected light can be diffracted for local Raman and fluorescence with additional fiber spectrometer.

The chemicals were purchased from Aldrich; Fuligo varians grew in the author's garden; styrene/acrylamide polymer latices were supplied by Prof. F. Galembeck, Instituto de Quimica, Universidade Estadual de Campinas, Brazil; fluorescent nanoparticles in polyvidone and dyed polyester fibers were from, Dr G. Wagenblast, Ludwigshafen, Germany; silver nanoparticles for SERS were from Dr. K. Kneipp, TU Berlin; the dolomite sample was from Dr. Th. Schöberl, Erich-Schmid Institut Leoben, Austria; the rabbit heart and shrimp eye preparations were supplied by Prof. P. Jaros, Universität Oldenburg, Germany; the human bladder cancer tissues from Charité Berlin, were prepared by Prof. G. Müller, LMT, TU Berlin, Germany, who also provided the blood bags; The dental alloys were from Dr. K. Liefeith, IBA Heiligenstadt, Germany.

Results and Discussion

The limits of light microscopy and STED

The possibilities of 3D-light microscopy (increasing the depth of focus at high resolution) may be demonstrated with the single cells of amoebae Fuligo varians at 5000:1 (on-screen) and focal step of 1 μm. Figure 3 shows at slightly enhanced natural color (for increased contrast) that every cell has a less colored nucleus, but further details of the nuclei are not resolved and confocal light microscopy would be limited to 200 nm resolution. We need thus much higher resolution for the local identification in the 10 nm resolution range for studying organelles in the nucleus that cannot be reached with hot aperture NSOM or stochastic techniques like STED, etc. but with apertureless shear force controlled SNOM.
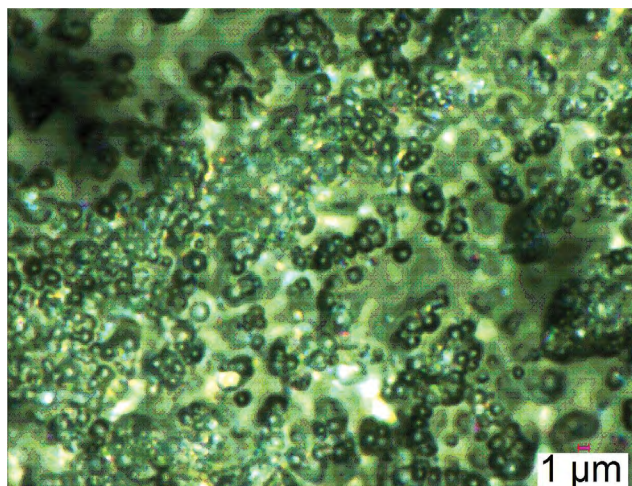

Figure 3: 3D microscopic image (red bar 1 μm, Z-range 3 μm) of *Fuligo varians*. These single amoeba cells aggregate and any one has one nucleus. The resolution limit of /2 is not reached here, but we would need reliable SNOM with the <10 nm resolution [1,12] for the resolution of further details.

Stochastic fluorescence techniques like STED (640 nm excitation, 755 nm depletion) with chemically changed nuclei would not be able to reach that goal. For example, the lateral resolution of STED as published from 8 Authors in a renowned journal [13] for cultured HeLa cells at Golgi (live or fixed) but selectively bound to the very complicated fluorescence dye Cer-SiH ($C_{68}H_{93}N_7O_8Si$, mw. 1169.65 D) molecules (17 authors in Ref. [14]) compares the common confocal line scanning with the corresponding "donat-light" STED scanning of the same sample. The half-widths at the narrowest point changed from 357 (or 317) to 175 nm by a factor of roughly 2. That is a remarkable but only slight sub-microscopic resolution. However, it is far away from the capabilities of the older apertureless SNOM technique that physically resolves below 8.6 nm [1,12,15]. Furthermore, the stochastic technique does not show the correct size or structural differences within the elongated fluorescence field instead of pristine HeLa-cells at Golgi as live or immobilized cells. Also the adjacent material is not detected, but covered by the fluorescence of the uncountable huge dye molecules.

The unexpected physical effect: reflectance enhancement in the shear force gap

The present author lectured and published since 1995 [4,6] on enhancement of the reflected light intensity abruptly when the shear force gap was reached. Such enhancement factors are 2 to >50. But surprisingly, the physicists group around J. Mlynek denied this valuable invention as non existing [2]. It turned however out, that these physicists were not able to prepare sharp enough tips (with 50-60 nm end radius that always broke) by etching with fluoric acid instead of pulling with commercial laser puller. After clarification of this controversy with Figure 4 [1,5], Keilmann's group used the enhancement for scattering type SNOM, however only for flat samples (but not daily life samples) by directing a laser focus directly to a dithering probe with the requirement for double modulation of the so scattered light both at the probe shaft and at the sample [16]. The apertureless reflection back to the fiber SNOM from 1995 measures materials dependent variations at the strongly enhanced level (chemical contrast). Approach curves with the horizontally vibrating tip (Figure 4) down to the shear force gap with sharp tip (R<20 nm) gives the unexpected enhancement of reflection back to the uncoated dielectric fiber tip. During the coarse approach low constant far-field stray-light is recorded. As soon as the damping starts the tip is mechanically lifted by 1 μm to keep it from penetrating into the surface. At the same time a near-field light flash is recorded by a scanner. From this height cautious close approach is started until the preset constant damping is reached and scanning is started at the enhanced signal level where different materials have different enhancement factors. Conversely, when a blunt or broken tip (e.g., an etched tip with end radius of 50-60 nm) is approached this does not give enhancement but a decrease of intensity when the shear force distance is reached [1,12,15], giving artificial response. That's why Mlynek failed, with the result that the present author's invention had a hard time for being acknowledged. Reliable SNOM relies on variations of the enhanced light with sharp tip. The constant far-field background does not destroy the contrast.

The damping influence

The enhancement effect depends on the tip sharpness and the amount of preset damping. The approach curve is linear at damping ranges without tip abrasion. One starts at reasonably low percentage and checks the radius before and after the last experiment. The middle of the linear range is a good choice, here at 55% damping in order to preserve the tip without abrasion and obtain good enhancement (Figure 5).
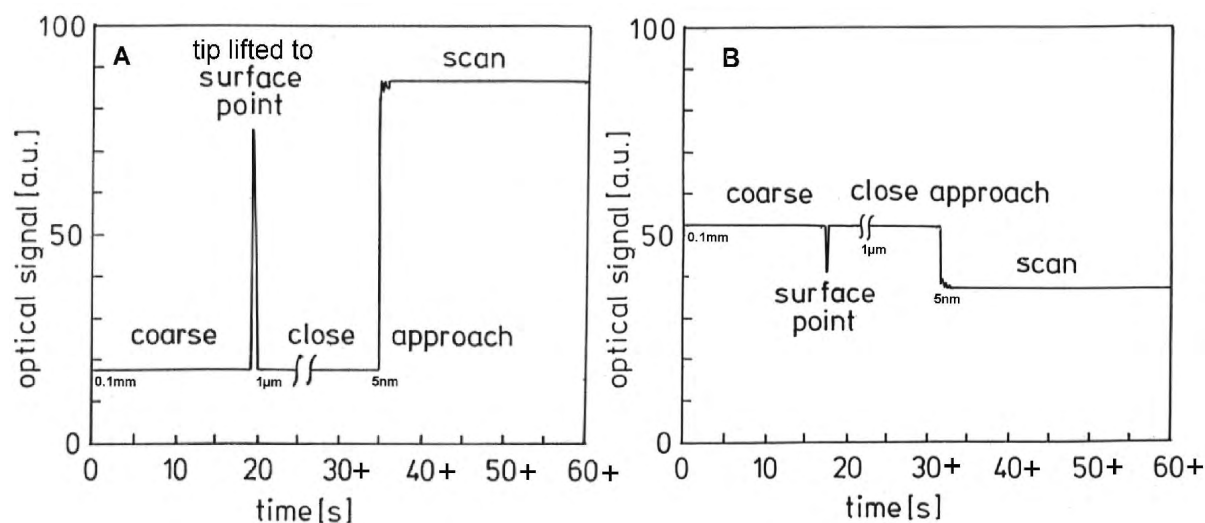
Figure 4: Rapid coarse and slow close approach curves down to the shear force damping gap; (A) with a sharp tapered quartz tip giving reflectance enhancement; (B) with a blunt tapered quartz tip giving intensity decrease; the tip is lifted by one µm when the damping of the tip vibration starts [1,12].

The sensitivities and enhancement factors vary strongly (2->50), so that chemical contrast is also obtained with closely related compounds (for example between isomers or biological sample constituents in organelles etc.). Also water layer (ambient humidity) and surface (hydr)oxides, or sulfides on gold and all sorts of dangling bonds on the daily life surfaces influence the shear force efficiency. Table 1 gives a short qualitative overview on the sensitivity of different materials. The reasons for the chemical contrast are also dependent on absorbance, emission, refractive index, molecular structure, polarity, and molecular packing. A useful chemical spectroscopy is obtained.

Table 1 shows that the variations in the sensitivity of the enhancement covers two powers of 10 and also the height of water layers plays an essential role. The new chemical spectroscopy is highly potent and there are already several examples with excellent contrast, including industrial applications. The variation is very large, which makes different materials distinguishable (chemical contrast).

The lateral resolution

The superior resolution power (<8.6 nm) of apertureless shear force SNOM has already been mentioned. Historically, aperture NSOM used more or less vertical steps as resolution standards, even though these must provide a topographic artifact but not SNOM. Gratings, spheres, and cubic crystals can be used for a rough preliminary check in particular to check the resolution power of SNOM probes (the sharper the better). Examples are latices (the aggregation phenomena are certainly also of interest for biological objects) or easily prepared cubes of NaCl by evaporation of its solutions on a glass slide. Figure 6 shows it sharply resolved. However this can only be a first indirect resolution guess.

Real resolution standards are based on chemical contrast and required for the final resolution power of shear force SNOM. For example, polishing of geode containing stones is continued until a more or less vertical solid interface is obtained, even when a nanoscale step cannot be avoided due to different polishing resistance. Figure 7 shows it on marble. Such interface even in the neighborhood of a residual marble elevation (that, of course, gives no SNOM contrast) is scanned and the cross-section along the chemical contrast line is

Material surface	F/% damping	Type of material
Anthracene (001)	0.0064	Organic, unpolar
Phthalimide with water layer	0.096	Organic, polar
Aluminium+Al$_2$O$_3$-layer+H$_2$O	0.025 (winter)	Metal with hydrated oxide
Aluminium+Al$_2$O$_3$-layer+H$_2$O	0.040 (summer)	Metal with hydrated oxide
Silicon+silica-layer+H$_2$O	0.373	Half-metal with hydrated oxide
Gold-SH	0.069 (winter)	Metal with S-H monolayer
Gold-SH	0.099 (summer)	Metal with S-H monolayer
Dolomite with water layer	0.265	Salt with water layer

Table 1: Near-field reflectance enhancement sensitivities (approach steepness) of various materials of different type [1,12].

analyzed. The original image obtained with a sharp tip that vibrated horizontal at right angle to the scan direction gives from top to zero 8.598 nm resolution. It would be much better (3.7 nm resolution) when the more commonly used 80 to 20% criterion were used [15]. We use in this review the 100 to 0% criterion of chemists.

Artifacts

Aperture NSOM suffers from essentially 8 types of artifacts that are avoided in apertureless shear force SNOM, as long as blunt and broken tips are excluded so that the near-field reflectance enhancement is present. Purposely executed scans with such unsuitable tips can reproduce such artifacts, which is very helpful in recognizing the invalid published aperture NSOM results. These are: topography imaging, interference rings contrast, stripes contrast at steep slopes, inverted derivative of topography, contrast inversion upon scan, inverted (wrong) contrast, displaced optical contrast, and local light concentration. Most prominent are interference fringes and (depending on the shape of broken tips) derivatives of the topography. Figure 8 shows 2 artificial examples [1,12,15,17]. They are not obtained in apertureless SNOM as long as the tips stay sharp, slopes are blow 70 or 80°, and energy control with an energy meter is performed.

Chemical contrast for solid-state mechanisms

The chemical contrast is not blurred by topography with all slopes below 70 or 80°. This is shown in Figure 9 with the topography of
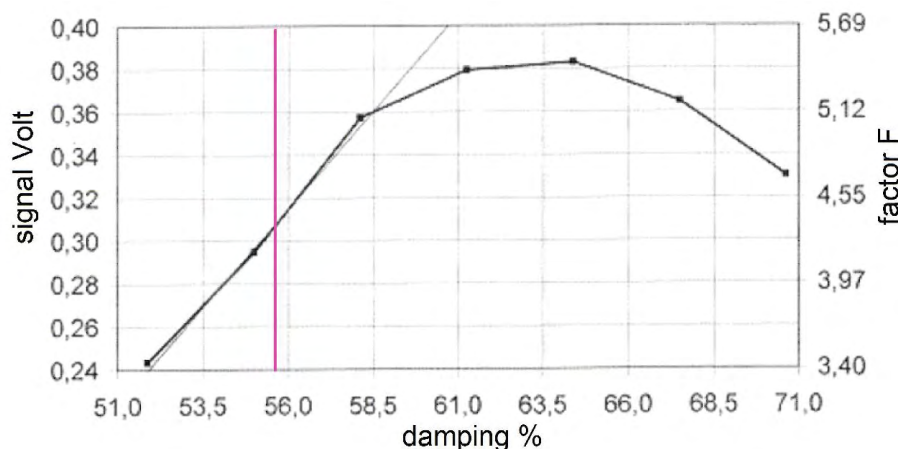
Figure 5: Approaches to dolomite (CaCO$_3$MgCO$_3$) showing linear dependence of the enhancement prior to tip abrasion in the bent part of the curve at too close damping distance; the sensitivity is ΔF/Δ% damping=0.265; the enhancement factor F=I/I$_0$ [1,12].
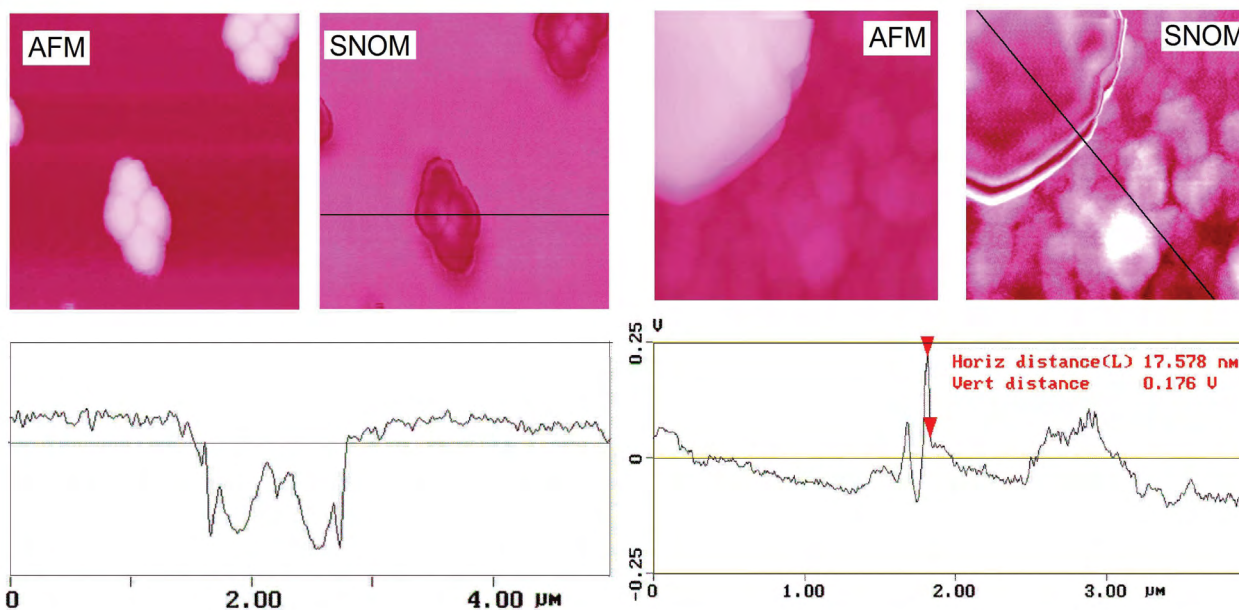

Figure 6: Left: styrene/acrylamide polymer latices (430 nm) give on both sides at the cross section a sharp depression as the tip has to pass a vertical on both sides. Right: sharper is the edge artifact at 1 µm vertical height of a sodium chloride cube on glass; this corresponds to <18 nm step-resolution of the sharp tip. Blunt tips give inferior step-resolution. Just dry a sodium chloride solution. These and others are simple tip checks [1,12].

4-nitro aniline, giving no SNOM contrast. Conversely, the topography that has been produced on initially flat 2-mercaptobenzothiazole on its (001)-face by autoxidation in air gives chemical SNOM contrast (2 mercapto S-H give S-S, less polar, thus less reflective). This proves the "island mechanism" by chemical reaction around defective sites on the actually non-reactive face (the single molecular layer protection of the (001)-face is thus slowly lost). True SNOM is, of course, always a chemical contrast.
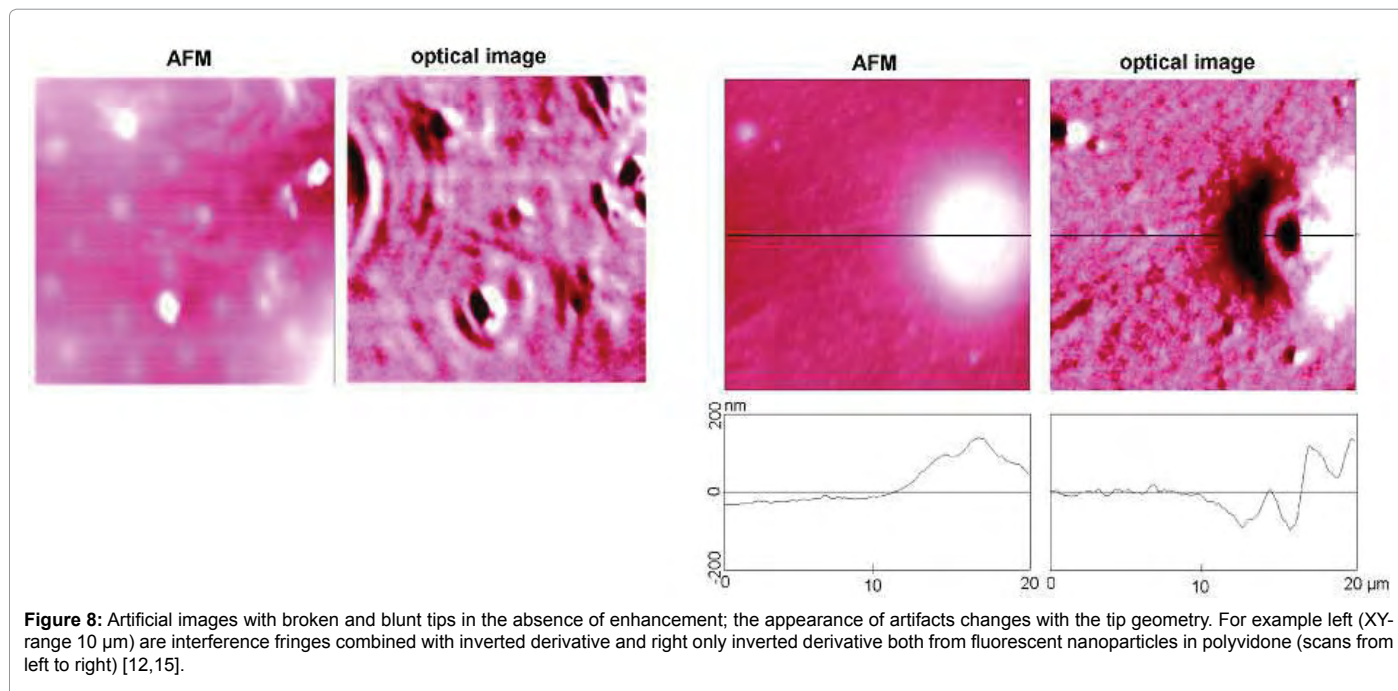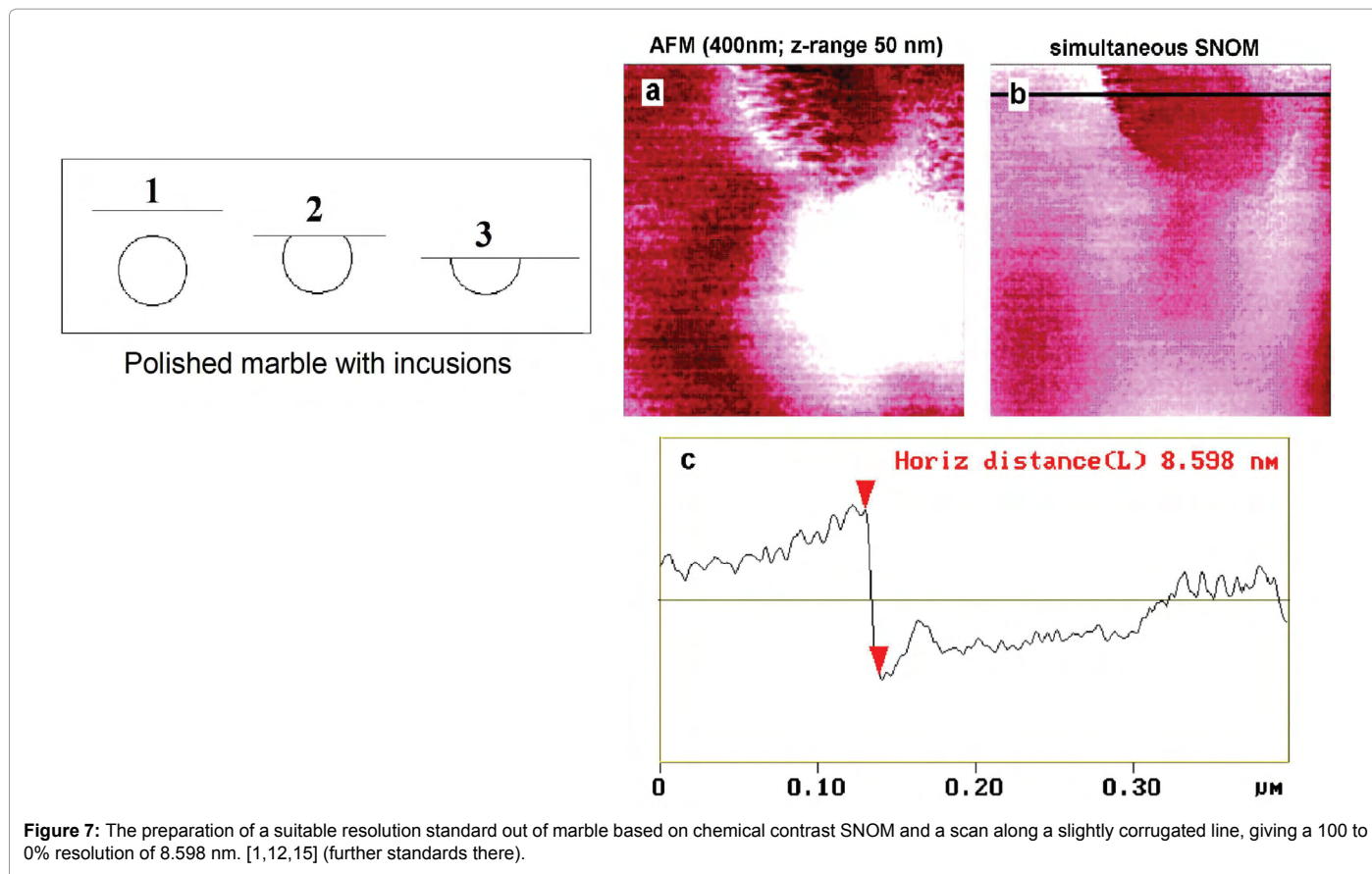
Another single molecular layer self protection towards autoxidation is encountered with anthracene. The overwhelming (001) face of the ordinary scales form remain >6 months unaffected in air. Similarly, the {110} face of the prism form has the anthracene of their long-side on top, presenting only its 9-position for reaction but not also the opposing 10 position that would be required for forming anthraquinone with oxygen (Figure 10). Conversely, both reaction sites are available on the crater slopes of the prisms, where autoxidation can occur. Thus, autoxidation is prevented by a single top layer on {110}, but it occurs at the slopes under it, although hardly seen by AFM. But the bright chemical contrast of SNOM reveals this surprising single molecular layer situation, as shown in Figure 10.

Similar solutions of mechanistic questions concerning single layer effects with sulfanilic acid are found in Ref. [12,15].
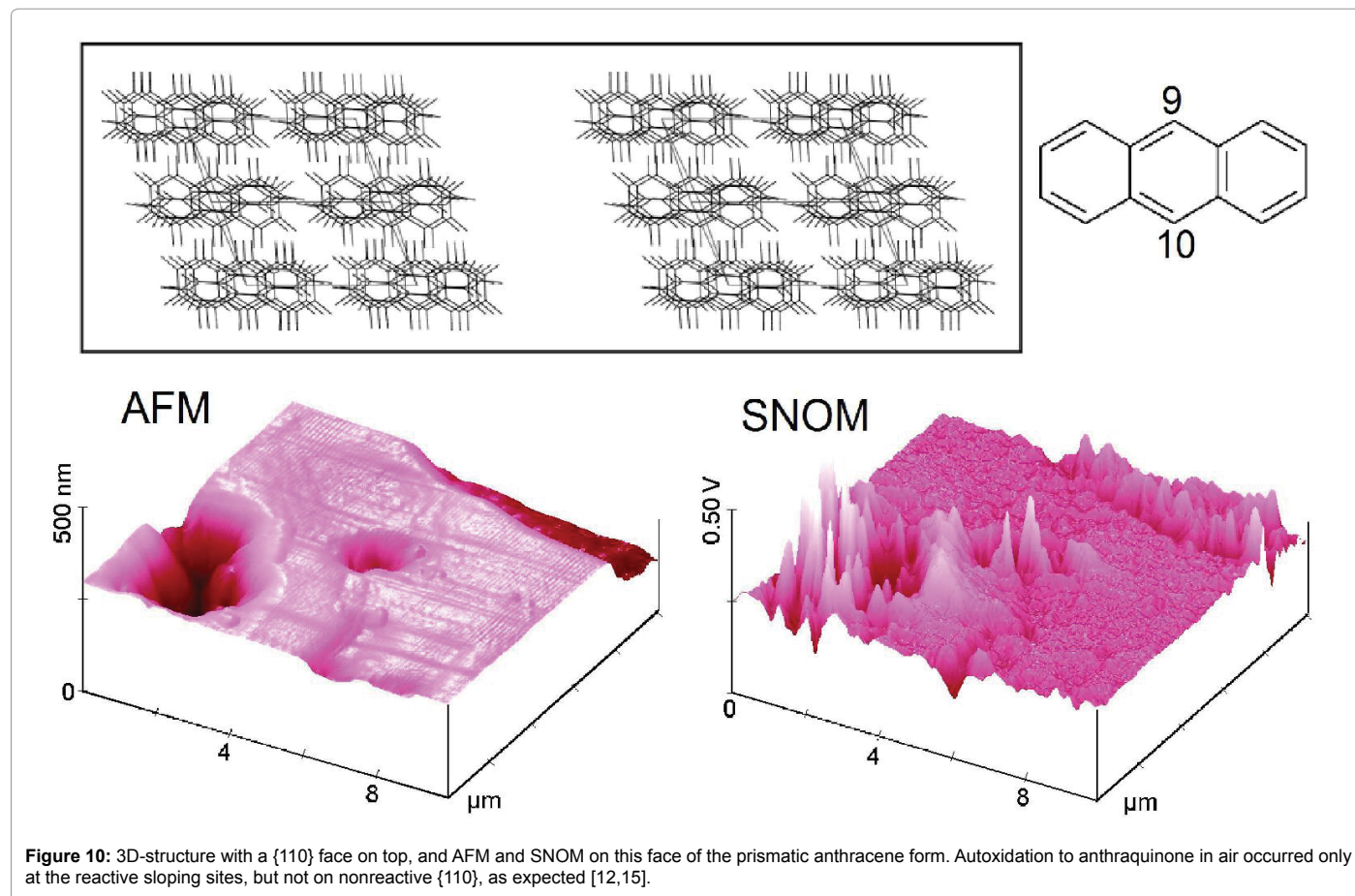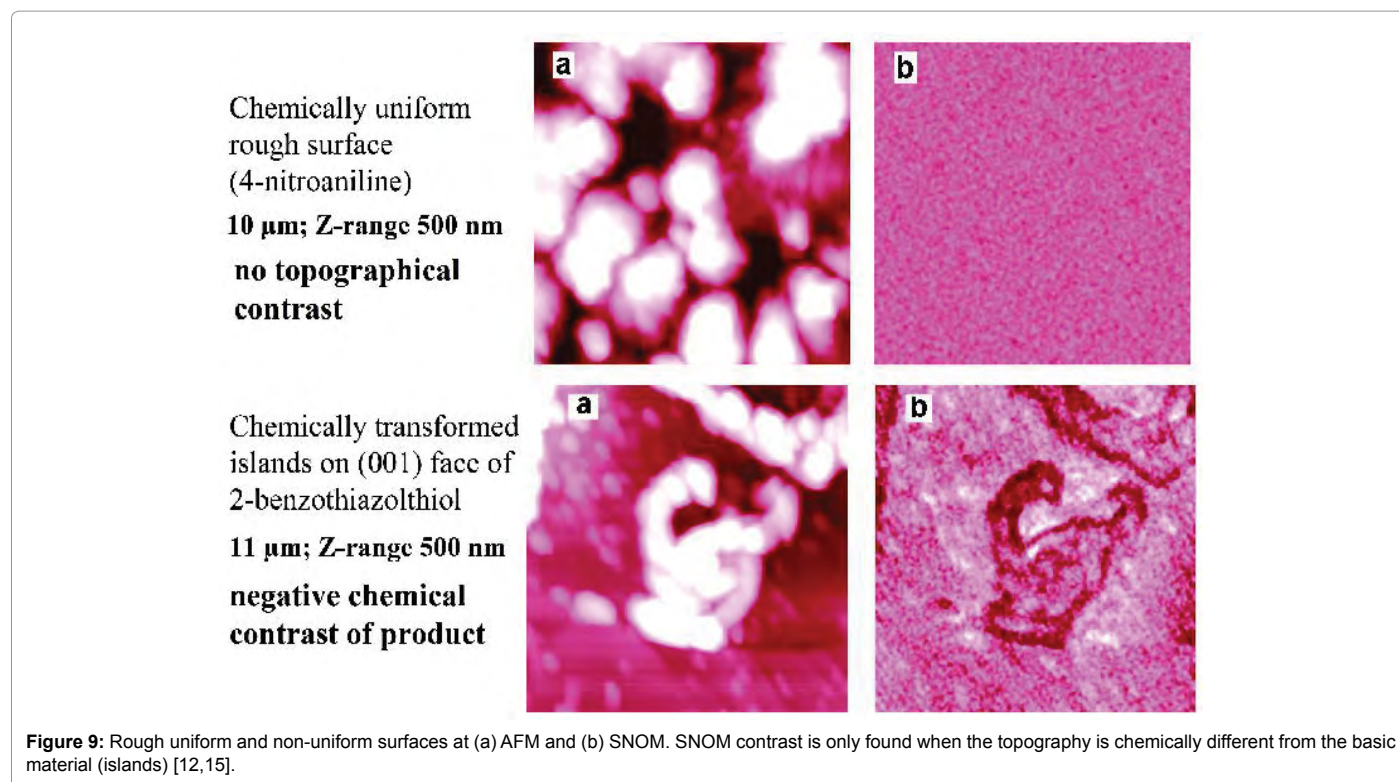
Localization and analysis of nanoparticles

Silver and gold nanoparticles are very important for enhancing

Figure 7: The preparation of a suitable resolution standard out of marble based on chemical contrast SNOM and a scan along a slightly corrugated line, giving a 100 to 0% resolution of 8.598 nm. [1,12,15] (further standards there).

Figure 8: Artificial images with broken and blunt tips in the absence of enhancement; the appearance of artifacts changes with the tip geometry. For example left (XY-range 10 μm) are interference fringes combined with inverted derivative and right only inverted derivative both from fluorescent nanoparticles in polyvidone (scans from left to right) [12,15].

Raman spectroscopy for chemical characterization. But their performance varies. Apertureless shear force SNOM images and characterizes them on a glass-slide. Figure 11 gives an example for a moderately effective silver sol. The chemical SNOM contrast is, of course, site specific. There are SERS (surface enhanced Raman spectroscopy) active bright, probably inactive silver particles, and dark silver oxide impurities (proof by local Raman SNOM).
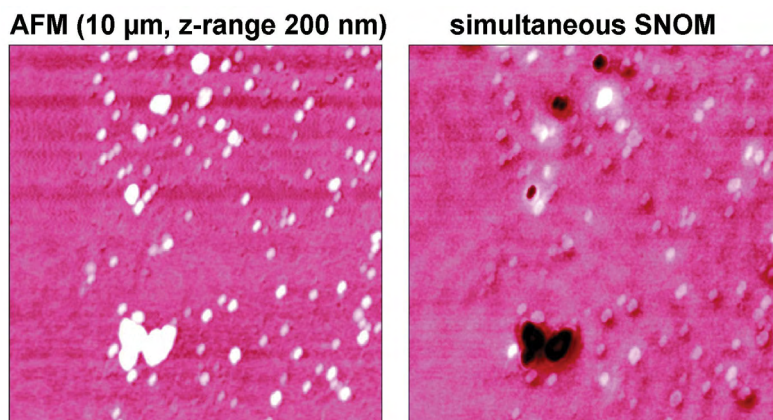
Figure 9: Rough uniform and non-uniform surfaces at (a) AFM and (b) SNOM. SNOM contrast is only found when the topography is chemically different from the basic material (islands) [12,15].

Figure 10: 3D-structure with a {110} face on top, and AFM and SNOM on this face of the prismatic anthracene form. Autoxidation to anthraquinone in air occurred only at the reactive sloping sites, but not on nonreactive {110}, as expected [12,15].

Figure 11: Concomitant AFM/apertureless SNOM of moderately SERS active silver particles [1,12,15,18].

Several other nanoparticles e.g., inactive gold ones were analyzed (In Ref. [12,15,18] with further images).

Local SNOM spectroscopy: SERS, Fluorescence and Raman

Local SERS SNOM spectroscopy with fiber optics: Very important is local SNOM spectroscopy for the identification of nanoscale objects. Local SERS enhancement with silver sols is further enhanced by shear force apertureless SNOM. The diffraction is achieved with a fiber spectrometer (service was provided by IFU GmbH, 09557 Flöha, Germany) as detector for the enhanced reflected light. For example 10 µl water containing 1 pg of adenine were dried together with Ag sol to a circle of 2 cm diameter. The local measurement in a 100×100 nm^2 area at a collection time of 10 min gave the prominent Raman spectrum of Figure 12 without curve flattening and without baseline subtraction at the correct 735 cm^{-1}. Applications for biological objects are suggested.

Local near-field Raman spectroscopy with fiber optics: A nanoscale area covered by the object in question is scanned as usual and the enhanced reflected light is diffracted with a fiber spectrometer. The performance is shown in Figure 13 with GaN (0001) on Al$_2$O$_3$ and scratched Si after 5 h re-oxidation to SiO$_2$ in moist air (data referred to in Ref. [12,15]). The collection time (488 nm) was 10 min and subtraction of the fiber's Raman signal was performed. Importantly, silicone is still detected despite the reformed SiO$_2$ layer. The points could have been closer set, but the Raman shift values correspond.

More important are local Raman SNOM identifications of unknown materials. The AFM on a polished natural dolomite surface in Figure 14 does not point to any peculiarities. However, the simultaneous apertureless SNOM contains a very bright area. Local Raman spectroscopy of the enhanced reflected light only from within that bright area with 145 scanlines at 488 nm using notch filter, light diffraction, and baseline correction gave the Raman response of pyrite (FeS$_2$), present as a geode.

This technique will be indispensable also for the identification of unknown (biological) objects that can be looked at due to their chemical differences and topographies. Also the analysis of glazed papers (including archeological ones) is one of the promising applications [12,15].

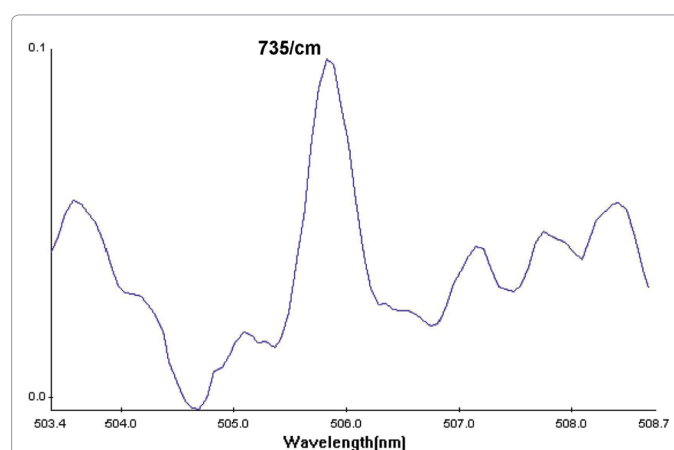## On-site enhanced fluorescence SNOM photo bleaching and

Figure 12: Local raw SERS SNOM of 140 thousand molecules Adenine in the presence of silver nanoparticles in 10 min [12,15,18].

diffusion coefficient calculation

The first indication that the reflected light does not only contain primary Rayleigh and Raman light provides an edge-filter (e.g., OG 515, Schott, >506) for 488 nm laser light. This has been used for the fluorescence analysis of a commercial nanoparticle dye in polyvidone resin. Figure 15 shows a remarkable difference between AFM and apertureless SNOM. The aggregation of particles (110-210 nm wide) is bent (the resin fills the void in the AFM) and the width of the single particles close to the surface is consistently 10 nm larger in the AFM than in the SNOM due to only 5 nm polyvidone cover (average width from larger scale images for statistics) with all consequences for color shading at car painting.

As in the case of local Raman Spectroscopy the light might also be diffracted with fiber spectrometer for recording of complete local fluorescence spectra.

Industrial fiber dyeing can go all the way through the fiber or only partly as with ring dyeing. The SNOM analysis requires embedding in a polymer with microtome cut. A through-dyeing of polyester fiber in Technovit resin (488 nm; edge filter OG 515: >506 nm; 200 µm s^{-1}) is shown in Figure 16. Importantly, the slopes do not give a SNOM response.

GaN: E1(TO): 560.8 cm^{-1}
E2:   570.4 cm^{-1}

Si: 519.7 cm^{-1}
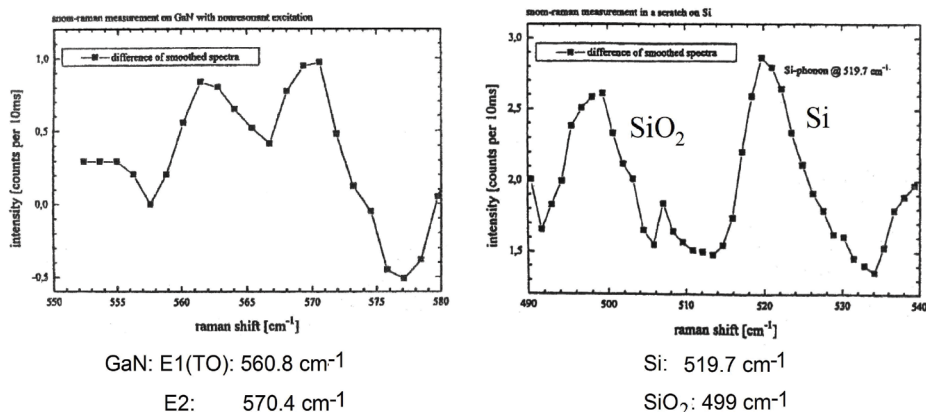SiO$_2$: 499 cm^{-1}

Figure 13: Local Raman SNOM spectra of GaN and silicon (in the scratch groove after 5 h).
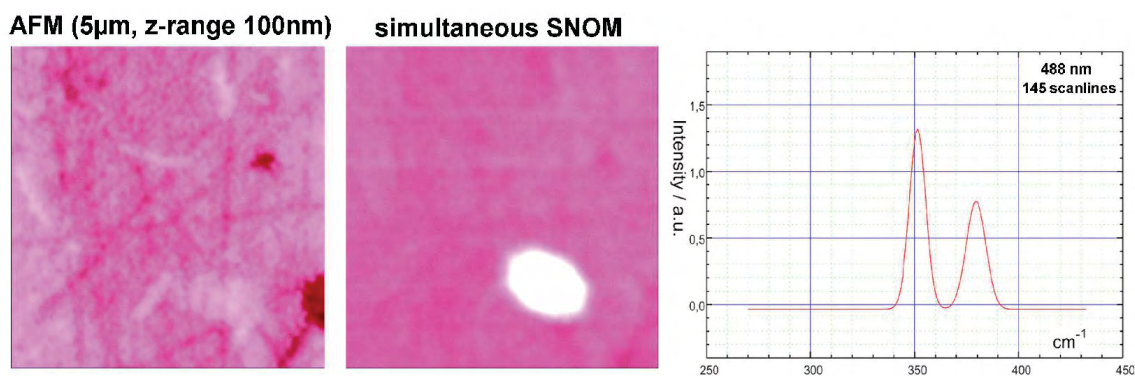

Figure 14: AFM, apertureless SNOM and local Raman spectrum indicating an unexpected pyrite geode in dolomite with the known line positions at the bright site invisible by AFM [1,12,15,18].
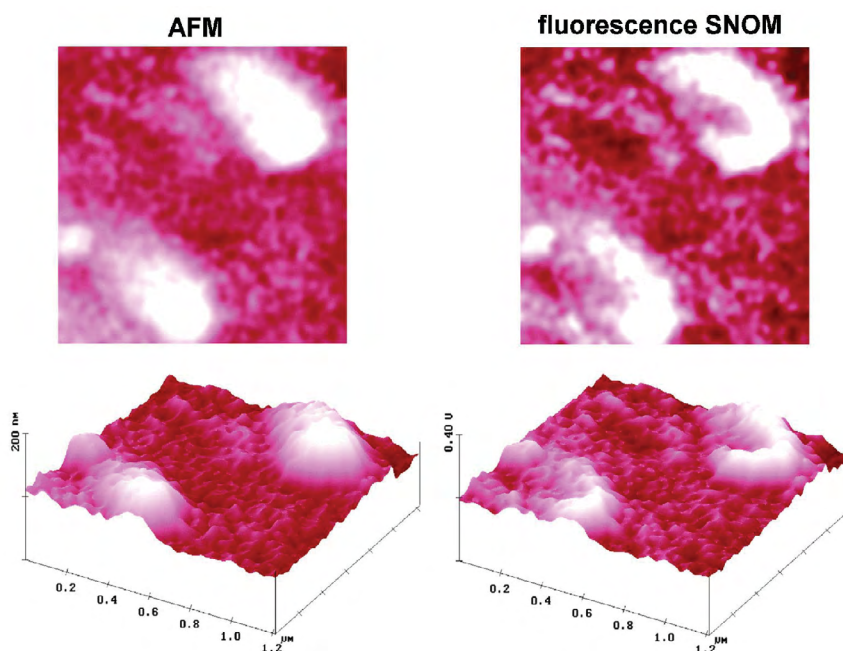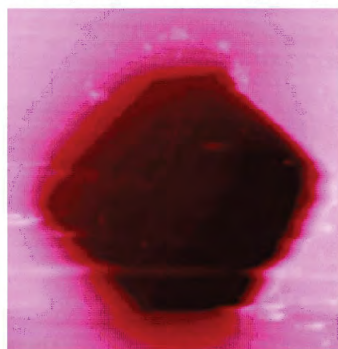

Figure 15: Apertureless SNOM fluorescence detection through cutoff filter of largely bent aggregating dye nanoparticles in polyvidone resin in 2-D and near perspective representation, showing also a single particle [12,15].
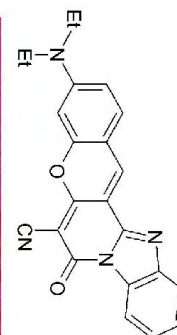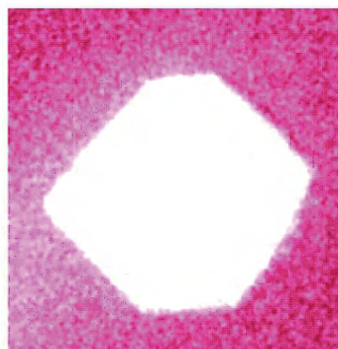
Figure 16: Simultaneous shear force AFM and SNOM of a technical fluorescent dye deep in polyester; through-dyeing is nicely secured by uniform SNOM fluorescence [12,15,19].

It is possible to test the photobleaching of through dyed fibers. Figure 17 gives an example. An evenly dyed polyester (microtome cut in Technovit 7100 resin) was scanned with the illuminated uncoated sharp SNOM tip (488 nm; 1.6 mW) in a 5 × 5 μm² area for 10 min, showing the photobleaching in a 6 × 6 μm² area. This result opens an important technical application for the relative on-site light fastness in the actual fabrics by large-scale apertureless SNOM. This dye is not perfect.

Partial ring-dyeing is often performed for saving dye, as with a polyester fiber microtome cut in Figure 18. The analysis technique is as above with another industrial dye (further examples in Ref. [12,15,19]). The fluorescence decreases exponentially from the outsides, and it is possible to calculate the diffusion coefficient most easily at the known dyeing temperature (130°C) and time (30 min), according to the common Fick's second law of diffusion. The result is here $D_{130°C}$=2.4 × 10^{-11} cm²s⁻¹, consistent with already known values, from very tedious determinations. Thus, our new technique is the easiest, fastest, and cheapest with enormous technical use, and broad biological/medical application prospects. So SNOM makes things easier. A fantastic application.

Apertureless SNOM for biological and medicinal tissues and objects

Chemical contrast in biological cells: Chemical contrast is most important for biological tissues. The application possibilities are legion. Figure 19 shows shear force scans on a not stained cryo-microtome cut of a rabbit heart ([12,15,18] with numerous further images at different sites). AFM shows the rather high topography but cannot alone identify the organelles. Such identification succeeds only with the chemical contrast of SNOM. Some of the features a through d have been attributed to organelles, primarily on their size and different chemical contrast, due to chemical differences. The chemical contrasts are very large indeed. The distinct SNOM scan can, of course, be much higher enlarged to resolve the detailed structure of the organelles. That should certainly be done by experienced cytologists and histologists with plant, animal and human cellular material, who are interested in unstained details at <8.6 nm resolution. This technique will undoubtedly be a valuable tool for cytology and histology.

Simultaneous shear force AFM (X and Y 5 μm, Z scale 2 μm) and apertureless SNOM images have been reported for an unstained shrimp eye in the peripheral region from a cryomicrotome. The less
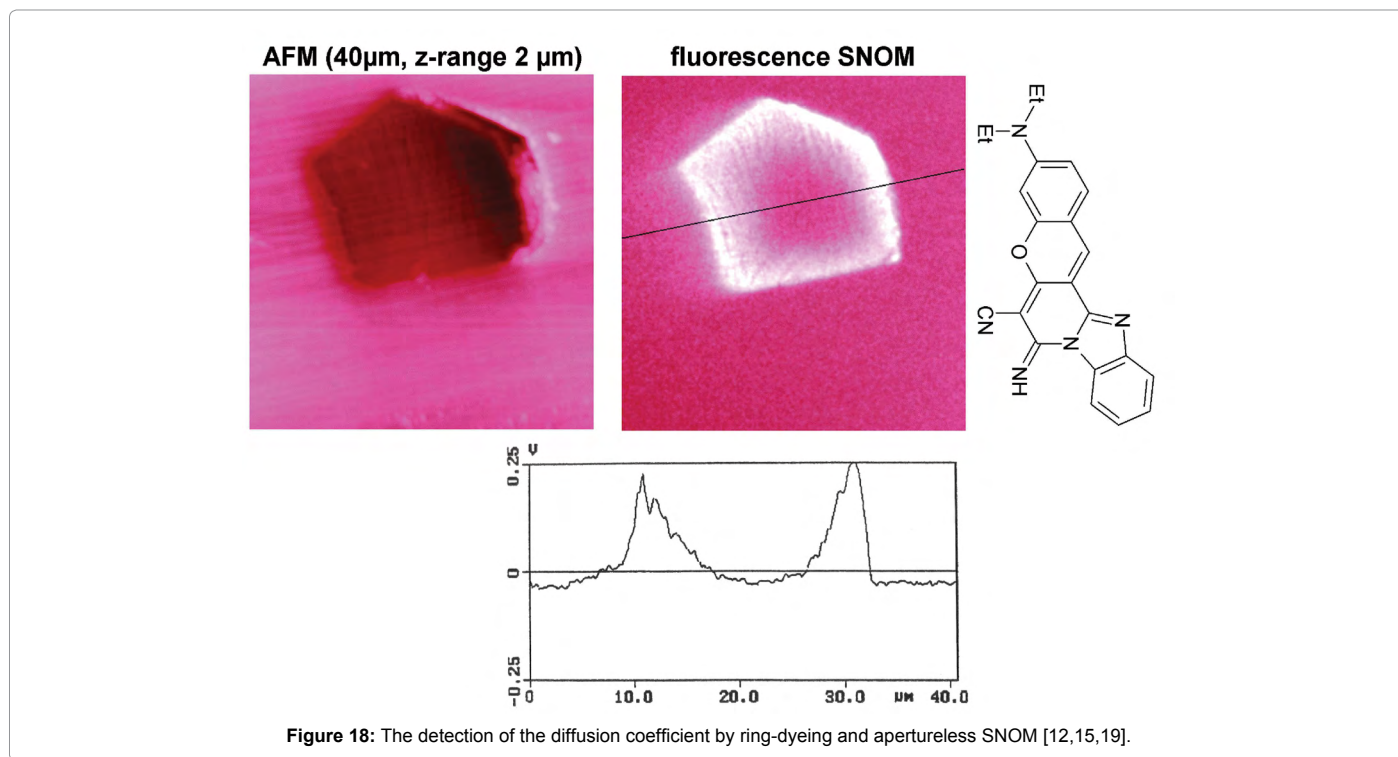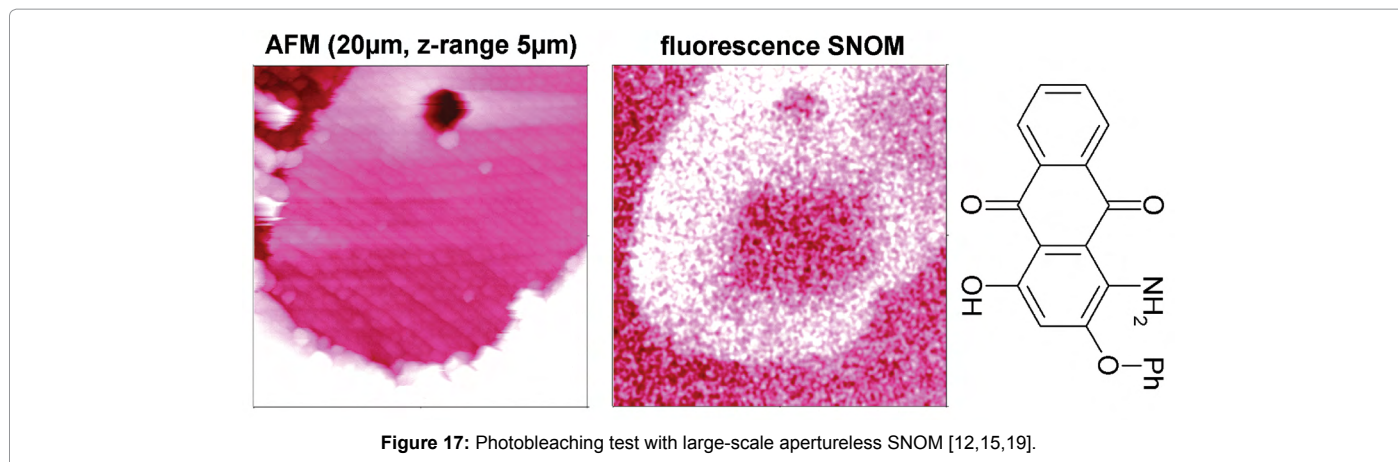
reflecting lysosome was further enlarged for resolving a series of (at lower level) bright, medium and dark suborganelle structures in Figure 20 [12,15,18]. SNOM distinguishes numerous arrays and single features within the lysosome and in its close environment. These are subject to interpretation and further enlargement for checking their structure elucidation at <8.6 nm resolution and enzymatic function analysis. This should certainly be very promising.

Cancer detection with apertureless SNOM

Cancer (pre)diagnosis is extremely important. Since cancer cells differ from the corresponding healthy cells of the same organ, the chemical contrast of apertureless SNOM is able to distinguish these. The necessary clinical material is always available via biopsy or upon surgery, where the removal of all cancerous material has to be histological controlled. The rapidly growing cancer cells require higher mineralization. Thus, a higher near-field reflection enhancement is expected than in healthy cells. This has indeed been shown in Figure 21 where the unstained cancerous and healthy iced cut (-10°C) and air-dried cancerous and healthy human bladder samples are compared (anonymous source from Charité Hospital, Berlin, Germany). These samples were scanned as large-scale simultaneous AFM and SNOM (X and Y at 25 and 20 μm). This was done at three as different as possible appearing sites each and compared Figure 21 [12,15,18].

The AFM images of healthy tissue show high roughness (various μm). The cancerous material appears to be somewhat finer structured, however a safe decision is hard to base on that, due to the high variety at the different sites. However, there are characteristic differences in the chemical contrasts of SNOM. The healthy material exhibits no pronounced or characteristic contrast at the different sites, independent of topography. Conversely, there is strong bright plate like contrast at all of the three different sites, without relation to the topography. This appears to be primarily due to the accumulation of metal salts in cancerous mitochondria at all of the different sites. Thus, a clear, safe, and sensitive distinction of cancerous and healthy tissue is achieved without staining.

Conversely, a trial to distinguish the commonly HE stained bladder materials was impossible. The staining wiped out all of the pertinent optical information giving almost no chemical contrast in the SNOM [12]. Rather the AFM surfaces were totally changed in 25 and 10 μm scans.

Figure 17: Photobleaching test with large-scale apertureless SNOM [12,15,19].

Figure 18: The detection of the diffusion coefficient by ring-dyeing and apertureless SNOM [12,15,19].

This tool should also work at various other rapidly growing cancers and it should be urgently used for breast cancer pre-diagnosis. The necessary biopsy is always available after suspect mammography results.

Apertureless shear force SNOM analysis of blood bag performance

The performance of blood bags for storage of human blood is an important and very big business. Why can the blood not longer be stored before serious deterioration? Clearly, the storage time depends on the material of the bag. Figure 22 shows that the AFM topography of a fresh common blood bag is rather high, but simultaneous SNOM at the purposely very rough site does not provide any chemical contrast, which proves its chemical uniformity. The AFM corrugation does not appear to significantly increase after some storage of human blood. At least no particularities are seen in the AFM at the now purposely

sought flatter site. However the bright chemical contrast in the SNOM shows that some deposition or reaction has occurred. It should now be investigated what the deposited material is, and learn how it could be impeded. Local Raman would be the first choice. It is hoped that the so gained information would help for increasing the blood storage times with improved materials using the new testing tools. Thus, the reliable and save SNOM has favorable potential for this very important practical application.

Apertureless SNOM for nanoscale checking of dental alloys

Dental alloys are checked according to standard electrochemical corrosion tests prior to admission for dentistry. Shear force apertureless SNOM should always check such admission at the nanoscale by comparing the alloys in a polished or molded state before and after the standard corrosion test, in order to exclude the risk of pitting that starts with nanopitting. The present technique is unique for such tests, while
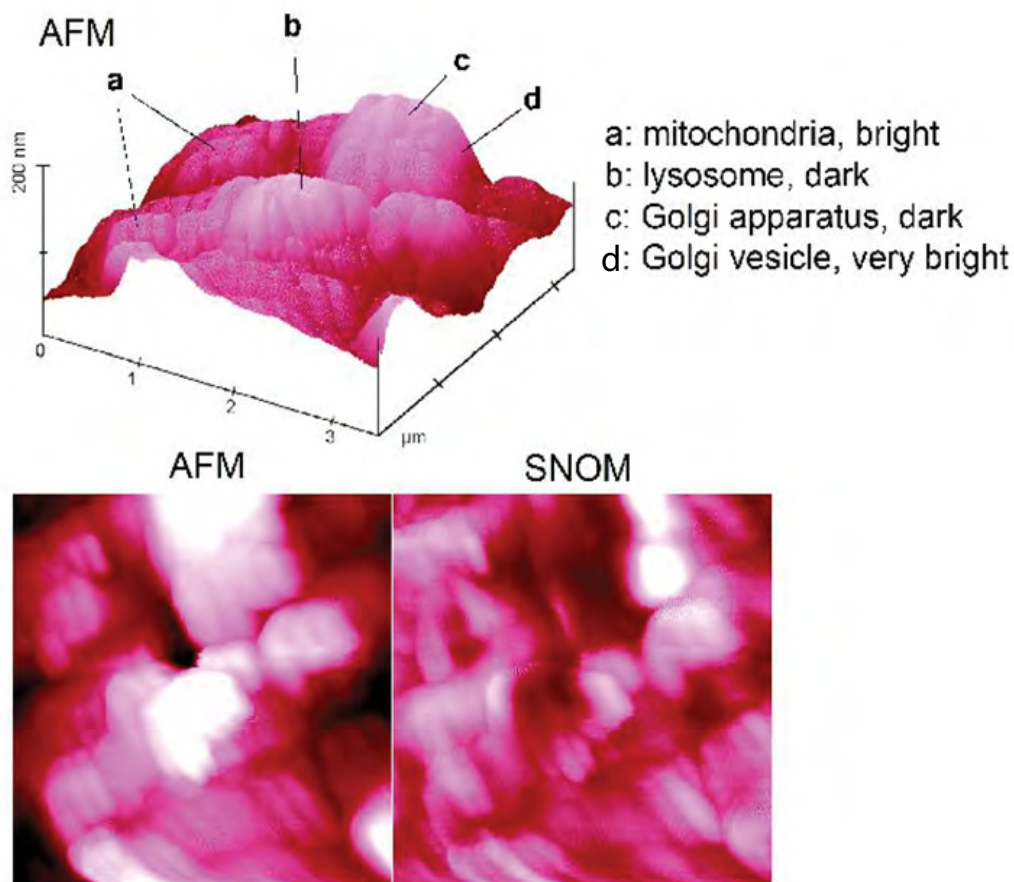
Figure 19: Simultaneous shear force AFM and apertureless SNOM images of an unstained cryo microtome of a rabbit heart showing topography and chemical contrasts, allowing some attributions to organelles [12,15,18].
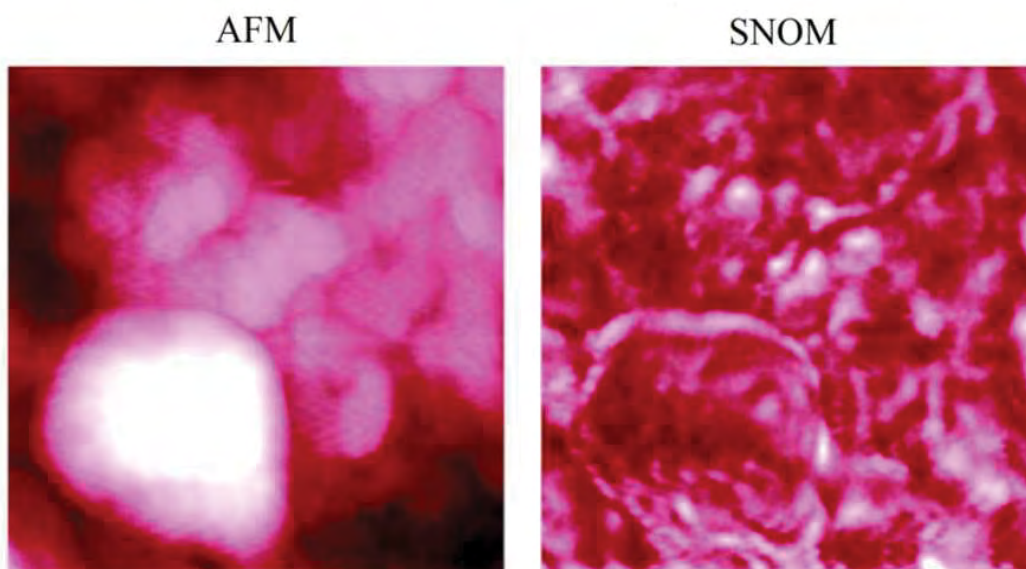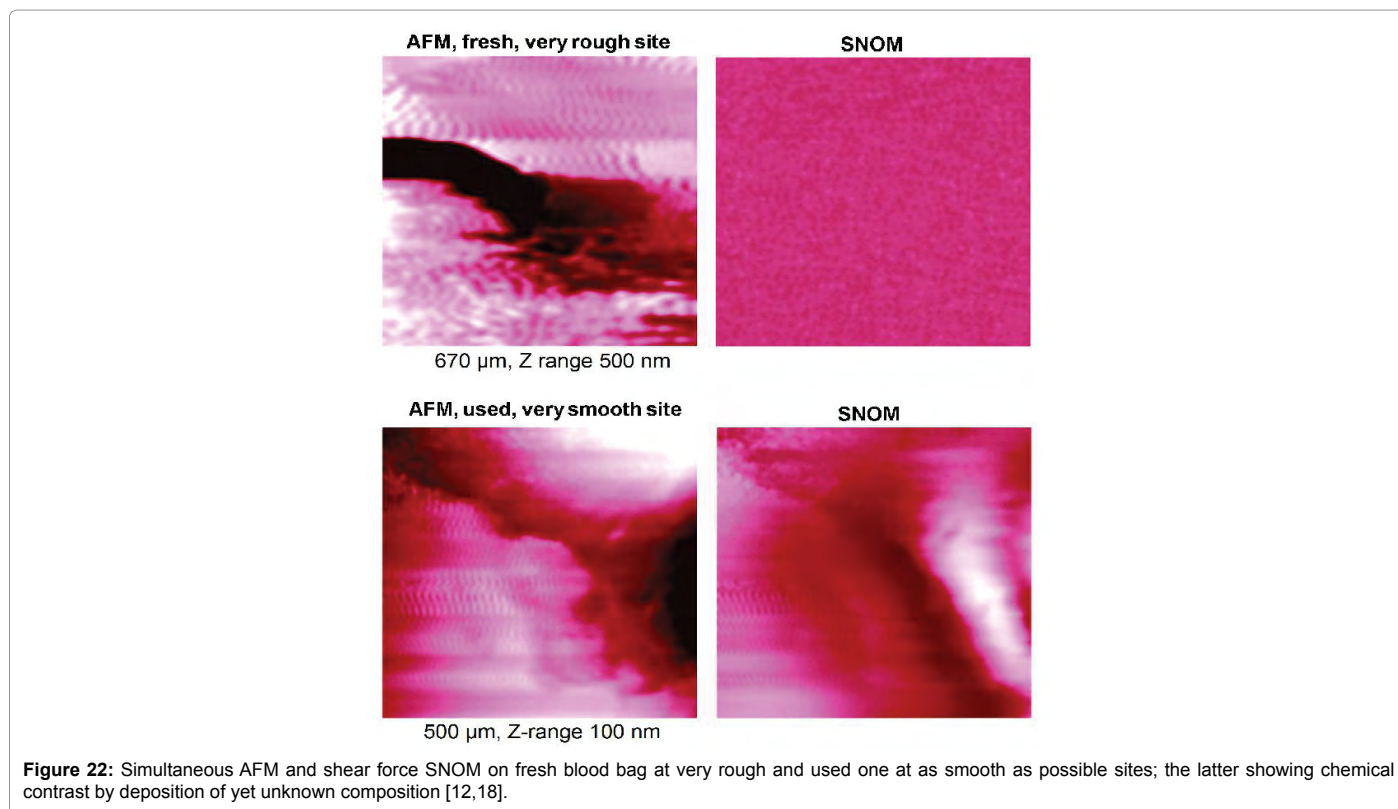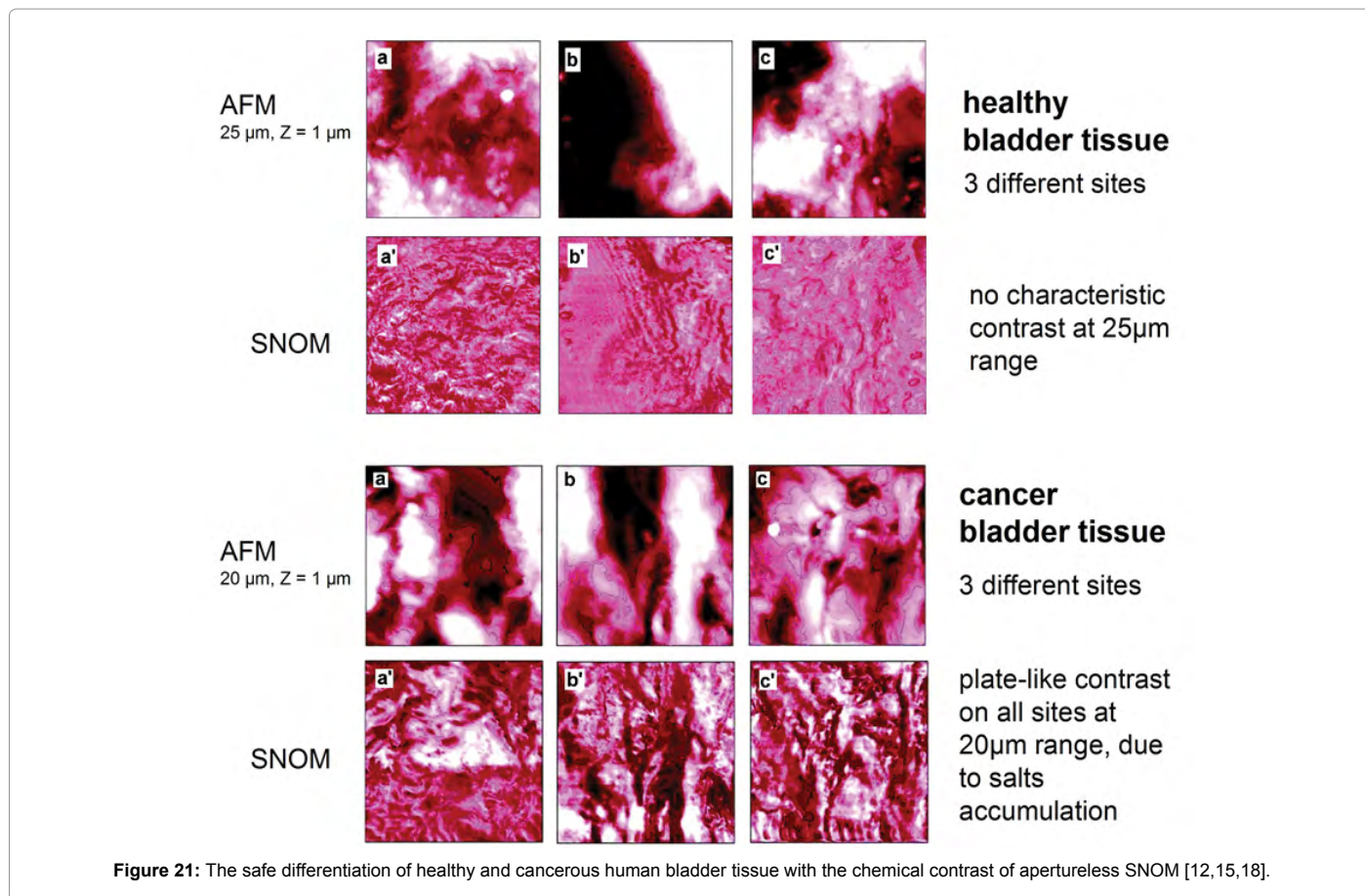

Figure 20: Simultaneous shear force AFM (X and Y 2.5 µm, Z-range 1 µm; pixel size 5 nm) and apertureless SNOM images of an unstained cryo-microtome of a shrimp eye lysosome, showing structured suborganelle structures, also in the close environment [12,15,18].

Figure 21: The safe differentiation of healthy and cancerous human bladder tissue with the chemical contrast of apertureless SNOM [12,15,18].

Figure 22: Simultaneous AFM and shear force SNOM on fresh blood bag at very rough and used one at as smooth as possible sites; the latter showing chemical contrast by deposition of yet unknown composition [12,18].

stochastic STED, PALM, STORM, etc. or XPS and other techniques fail. Numerous already admitted dental alloys were "blindly" tested and classified. Only three of them covering the types of observation can be treated here, as reported in [18]. Further data that are industrially used, must not be disclosed. The names or composition of the alloys are not even known to the present author who guided the investigations within the BMFT project. Most of the alloys proved safe, giving smooth uniform corrosion without chemical contrast, excluding local formation of galvanic nano elements. Thus, when chemical differences between metals or metallic alloys form upon corrosion, such dental alloy must be retracted from the market and replaced from the teeth, notwithstanding the question of the corrosion rate that has also been judged at non-pitting ones.

Alloy (A) (cobalt containing) is supplied with the steep abrasion edges how the dentist uses it. Figure 23 shows the AFM (a) and the steep slopes' edge artifact of SNOM (b) (cf. Figure 6) without chemical contrast. After the electrochemical corrosion, the surface is still edged in the AFM (c) and protrusions are on it, but there is no chemical contrast in the SNOM image (d). No nano pitting is found and this alloy is safe in that respect.

Alloy (B) (containing copper) behaves different upon electrochemical corrosion (Figure 24). Before corrosion AFM (a) and SNOM (b) reflect the typically abraded steep sharp edges. The hill on (a) is an impurity as shown by the dark chemical contrast in (b). After corrosion the AFM (c) is rather smooth and it lost all of the edges and the impurity. The SNOM (d) without chemical contrast excludes nanopitting and this is thus a safe alloy in that respect.

Alloy (C) contains nickel. It was supplied to the dentists with the typical steep abrasion edges, as dentists used it. Figure 25 shows the AFM (a) and the steep slopes artifact of SOM without chemical contrast (b). After the electrochemical corrosion the AFM has deep craters and the simultaneous SNOM exhibits chemical contrast at their sites. That means, we have nanoscale galvanic elements there, leading to nano pitting corrosion that would grow further and further, as local galvanic elements were formed. This alloy is therefore very dangerous for dentistry. Immediately after the images of Figure 25 were obtained, an urgent phone call achieved withdrawal of this dental alloy for the safety of the patients. The risk with this alloy was not known before and could not be found with other techniques [18]. Thus, shear force apertureless SNOM is also an indispensable and cheap technique for rapid detection of metal alloy pitting, starting at the nanoscale. It should thus be acknowledged and supported as an important state-of-the-art, but not forgotten by the present hype with stochastic [3].

It should be noted that such measurements are state of the art now. Everybody having the wrong dental alloy in his/her mouth can claim remedy, if necessary.

Conclusion

A revival of the simplest and most economic apertureless SNOM, providing interpretable results for real-world samples is described. The most reliable apertureless shear force SNOM concomitant with AFM is physically sound established (technique, strongly enhanced near-field reflection back to the illuminating quartz tip, chemical contrast, physical mechanism, <8.6 nm resolution, nanotechniques, artifacts' avoidance, local nano-spectroscopy, SERS, Raman, local sample fluorescence). The very diverse and important applications deserve revival and extensions of its use. Reasons why this might have been less supported in the past are manifold. First of all the strange denial by not acknowledging the technical basics by physicists [2] hampered the broader development. Then there was the continuing hype with tuning-fork feedback being unduly slow for useful scanning rates instead of using He/Ne-laser light as feedback trigger, permitting fast scanning. And finally the hype with the stochastic techniques [3] with
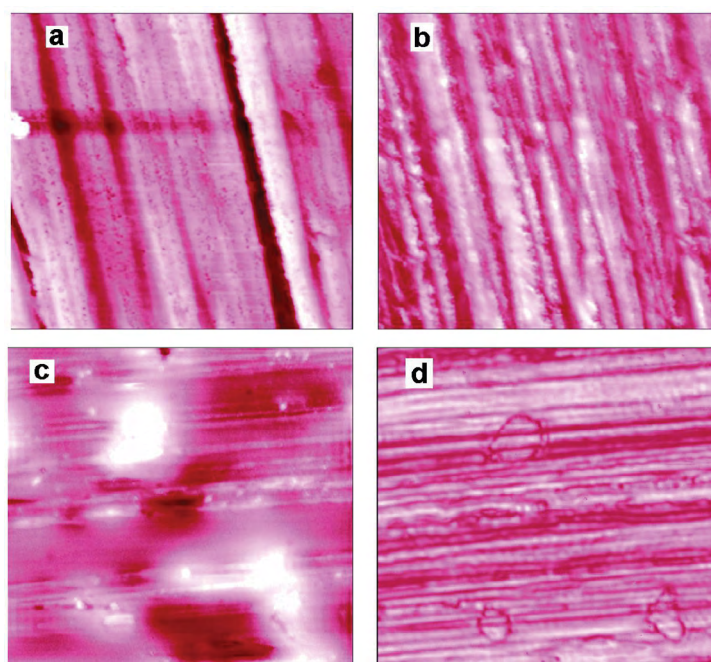

Figure 23: Simultaneous shear force AFM of alloy (A); (a) before (10 µm, Z-range 1 µm) and (c) after electrochemical corrosion (10 µm, Z-range 600 nm). The corresponding SNOM images are (b) and (d), respectively [12,18].
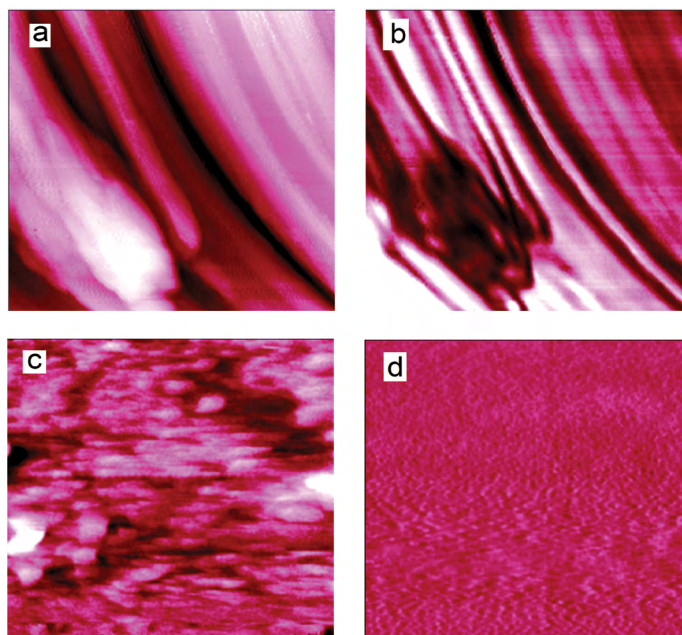
Figure 24: Simultaneous shear force AFM (10 µm, Z-range 400 nm) of alloy (B); (a) before and (c) flattened after electrochemical corrosion. The corresponding SNOM images are (b) and (d), respectively [12,18].
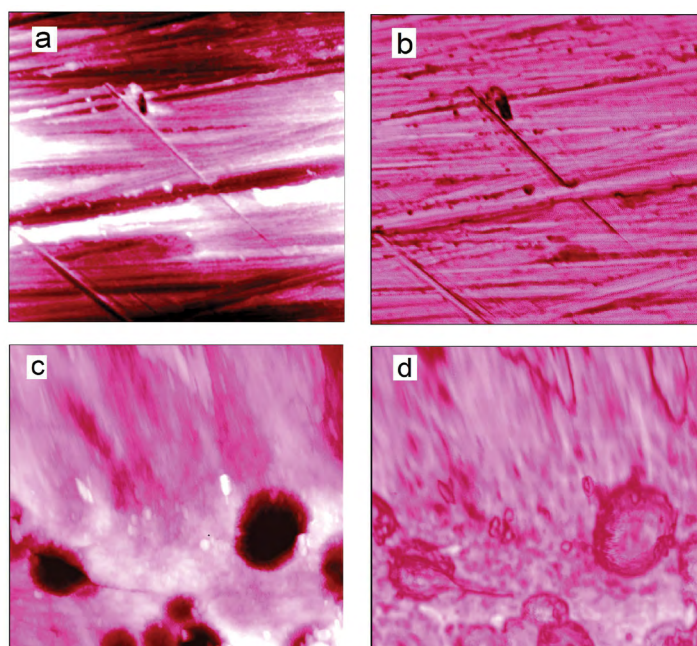

Figure 25: Simultaneous shear force AFM of alloy (C); (a) before (10 µm, Z-range 300 nm) and (c) after electrochemical corrosion (10 µm, Z-range 1.6 µm). The corresponding SNOM images are (b) and (d), respectively [12,15,18].

their very limited versatility that are extremely more complicated in design, expertise and cost, though at the expense of chemical alteration of biological materials by connecting to huge fluorescence dyes with very much inferior resolution of fluorescence maps of the latter, instead of scanning the unchanged material itself. Thus, the well preceding cheap and simple, easy to operate apertureless shear force SNOM must now be used for countercheck (unavoidably with the creation of new improved knowledge) of all conclusions from the poorly sub-microscopic resolved data of stochastic STED, STORM, PALM, etc. with highly restricted versatility, missing most important facts. Apertureless SNOM is able to resolve the underlying natural biological objects (and their cellular environment) without staining at much much more detail with <8.6 nm resolution. A particular advantage of well-done apertureless SNOM is its huge versatility. All

types of solid surfaces, in particular soft and hard biological/medicinal ones, can be directly studied at unparalleled optical resolution, and also µm height ranges can be rapidly artifact-free scanned up to slopes of 70 or 80°. This has been shown with academic and real-world samples including various industrial applications from organics, inorganics, nanoparticles, tissue dyeing, diffusion coefficients, dental alloys, local SNOM spectroscopy, chemical detection with local Raman, blood bags, well distinguished organic cell constituents, suborganelle details, cancer detection in human tissue, etc. Nothing of that is available from STED, PALM, STORM, etc.

It is expected that the results with shear force apertureless SNOM by enhanced reflection back to the fiber for flat and rough (including industrial) surfaces shall also officially be declared as state-of-the-art. Knowledge on it deserves public spreading of these facts and new funding. Unfortunately, that is not facilitated by the present hype with more recent stochastic techniques (STED, PALM, STORM, etc. [3]) that are not able to tackle such practically important submicroscopic tasks, despite their excessive complexity and costs.

Acknowledgements

References

1. Kaupp G (2002) Research Report of the German Bundesministerium für Bildung und Forschung BMBF (1999-2002), FKZ 13N7640/3: obtainable from Technische Informations bibliothek, Deutsche Forschungsberichte, Welfengarten 1B, Hannover, Germany.

2. Sandoghdar V, Wegschneider S, Krausch G, Mlynek J (1997) Reflection scanning near-field microscopy with uncoated fiber tips: How good is the resolution really?. J Appl Phys 81: 2499-2503.

3. Nobel Prize for Chemistry (2015).

4. Kaupp G (1995) AFM and STM in photochemistry including photon tunneling. Adv Photochem 19: 119-178.

5. Kaupp G (1996) Optical nearfield microscopy, chemical contrast with cold tips. Lecture at the INCOM Düsseldorf: March 3.

6. Kaupp G (1996) Supermicroscopy in supramolecular chemistry: AFM, SNOM, and SXM in Comprehensive Supramolecular Chem 8: 381-423.

7. Kaupp G, Herrmann A, Haak M (1997) Near-field optical microscopy with uncoated tips: Calibration, chemical contrast on organic crystals, and photolithography. J Vac Sci B 15: 1521-1526.

8. Kaupp G, Herrmann A (1997) Chemical contrast in scanning near-field optical microscopy. J Phys Org Chem 10: 675-679.

9. Kaupp G, Herrmann A (1999) SNOM by near-field reflectance enhancement: a versatile and valid technique. J Phys Org Chem 12: 141-143.

10. Kaupp G, Herrmann A, Haak M (1999) SNOM, a genuine photochemical technique. Internet Photochem Photobiol.

11. Kaupp G, Herrmann A, Schmeyers J, Boy J (2001) SNOM a new photophysical tool. J Photochem Photobiol A 139: 93-96.

12. Kaupp G (2006) Atomic Force Microscopy, Scanning Nearfield Optical Microscopy and Nanoscratching, Application to Rough and Natural Surfaces, Springer.

13. Toomre D, Schepartz A, Erdmann RS (2014) Super-resolution imaging of the Golgi in live cells with a bioorthogonal ceramide probe. Angew Chem 53: 10242-10246.

14. Lukinavicius G, Reymond L, Johnsson K (2014) Fluorogenic probes for live-cell imaging of the cytoskeleton. Nature Methods 11: 731-733.

15. Kaupp G (2012) Scanning Near-Field Optical Microscopy (SNOM), in Supramolecular Chemistry: from Molecules to Nanomaterials. Steed JW, Gale PA (eds.), John Wiley and Sons Ltd., Chichester, UK 2: 669-687.

16. Knoll B, Keilmann F (2000) Enhanced dielectric contrast in scattering-type scanning near-field optical microscopy. Opt Commun 182: 321-328.

17. Kaupp G (1999) Artifacts in scanning near-field optical microscopy (SNOM) due to deficient tips. J Phys Org Chem 12: 797-807.

18. Kaupp G, Herrmann A, Naimi-Jamal MR (2003) Research Report (1999-2002) of the German Bundesministerium für Bildung und Forschung BMBF, FKZ 13N7519: obtainable from Technische Informationsbibliothek, Deutsche Forschungsberichte, Welfengarten 1B, Hannover, Germany.

19. Kaupp G, Herrmann A, Wagenblast G (1999) Scanning near-field optical microscopy (SNOM) with uncoated tips: applications in fluorescence techniques and Raman spectroscopy. Proceedings of Spie-The International Society for Optical Engineering (1999), 3607(Scanning and Force Microscopies for Biomedical Applications)